System Analysis for "Sharp-Edge" Re-entry Vehicles

Ingrid Dietlein[1] and Alexander Kopp[2]
Deutsches Zentrum für Luft- u. Raumfahrt e.V., Institute of Space Systems, Bremen, Germany, 28359

Sharp-edged geometries for unmanned re-entry bodies are currently under investigation at DLR. During the phase 0 study an initial design for such a vehicle is developed. This paper presents the state of work in the design and describes briefly the process. The focus will be laid upon re-entry trajectories, aerodynamics and trimming as much as upon analysis of mass and centre of gravity.

Nomenclature

AoA	=	Angle of attack
CoG	=	Centre of gravity
L/D	=	Lift-to-drag ratio
OMS	=	Orbital manoeuvring system
Ma	=	Mach number
MECO	=	Main engine cut-off
RCS	=	Reaction control system
TPS	=	Thermal protection system

I. Introduction

DURING re-entry of a vehicle from space the high kinetic energy resulting from high orbital velocities has to be dissipated. This is accomplished by exploiting aerodynamic drag during the flight through the atmosphere. This comes at the cost of significant heat loads on the vehicle.

In order to keep heat loads low most re-entry vehicles are formed as blunt bodies resulting in rather low lift-to-drag ratios (L/D). Much of the heat energy remains in the flow and is not transferred to the body. High pressure resistance and detached shock waves characterize this type of vehicles. Well known examples of such blunt bodies are the Apollo and Soyuz capsules but also winged bodies such as the Space Shuttle behave like blunt bodies since flown at high angles of attack.

Blunt bodies show some drawbacks despite being the predominant shape for re-entry vehicles. One major drawback is the highly reduced downrange and crossrange due to the comparatively low lift-to-drag ratio. The time frame for re-entry is very tight and mission flexibility is reduced as a direct consequence because an adequate landing site has to be in reach of the vehicle. Furthermore, the curved shapes of the Thermal Protection System (TPS) lead to increased effort in development, production and a high number of tiles. Therefore the ease of reusability is considerably reduced as production of these tiles is complex and linked to high cost.

Sharp-edged facetted shapes can circumvent these drawbacks by using flat tiles. This kind of shapes is composed of several flat tiles, each one of them characterized by a large area and constant thickness significantly reducing the production and development effort. Furthermore, if flown at small angles of attack with the formation of an attached shock wave high lift-to-drag ratios become available. This results in a significant increase of downrange and most importantly of crossrange when compared to a blunt body. It opens access to landing latitudes not available to blunt bodies with low lift-to-drag ratios due to their limited crossrange capability.

The benefits from a sharp-edged vehicle with a high lift-to-drag ratio are currently examined by DLR within the project REX Free Flyer. For this project DLR can revert to considerable experiences with this technology gained from the sharp-edged suborbital re-entry vehicles SHEFEX.

[1] System Engineer, System Analysis for Space Transportation, Robert-Hooke-Str. 7, 28359 Bremen, Germany
[2] System Engineer, System Analysis for Space Transportation, Robert-Hooke-Str. 7, 28359 Bremen, Germany

The operative REX Free Flyer is a sharp-edged re-entry vehicle conceived to present to scientists an in-orbit experimental platform for research in a microgravity environment which allows retrieving the experiments after re-entry. The vehicle itself shall be reusable in large parts. The nose with ablative thermal protection system and some expendable parts like the canopy protecting the parachute system for descent are not reusable in the current design.

During the on-going phase 0 study, different vehicle configurations were examined on a system level. From a large scale of configurations one as the baseline configuration for further studies has been chosen after several iteration steps. This paper presents the accomplished work and the chosen configuration for the current state of work.

II. Reference Mission and Launch Vehicle

For this study a generic mission was defined in order to obtain a generic vehicle design as the starting point for further in-depth examinations. The VEGA launcher was chosen as the generic reference launcher since its payload capacity complies well with the requirements for the REX Free Flyer. Other launch vehicles may be considered, too, though, provided that sufficient payload and payload volume capacity can be offered.

The baseline concept for the REX Free Flyer mission is designed to allow landing in Australia. Therefore an orbit with an inclination of 30° was chosen as the reference orbit. Its altitude was fixed to 300 km and its shape to being circular. The in-orbit time is scheduled to be 200 minutes corresponding to approximately two orbital revolutions. The final descent will be accomplished with the help of an adequately designed parachute system.

The currently available user manual of the VEGA launch vehicle[2] shows an available payload mass of approximately 2200 kg for the target orbit and allows for payloads of 5.5 m length and 2.38 m width.

The baseline concept is designed to attribute autonomous de-orbiting capability to the vehicle but a de-orbiting by the VEGA upper stage AVUM may be envisaged.

As far as possible the standard payload adapter shall be used in order to circumvent a dedicated development of such a device. This requires the interface structure to be designed accordingly.

Furthermore the following requirements have to be met by the vehicle and the mission design:

1) The re-entry trajectory shall avoid skipping manoeuvres in order to allow for the employment of well known GNC principles without accepting large deviations.
2) Lift-to-drag ratio shall be equal or superior to that of the Space Shuttle, i.e. equal or superior to 1.2.
3) The ability to trim the vehicle during supersonic flight has to be guaranteed. Though aerodynamic stability is desired it is not required.
4) The maximum allowable internal temperature was fixed to 70°C in order to protect the electronic hardware from damage. It is assumed that the payload container is appropriately insulated in order to protect the experiments. First thermal analyses indicate that this temperature is not reached before several hours after landing.
5) The payload mass including the mass of its own power supply is fixed to 120 kg. The payload shall be placed within a standardized container.
6) The overall mass of the vehicle shall not exceed 1500 kg.

III. Approach and Assumptions

More than 20 different vehicle configurations were examined and evaluated on system level. These configurations differ mainly in external shape which was varied in a systematically way. Parameters for variations among others were the width, the length and nose angle. One family of geometries developed in the frame of this study had been inspired by geometries studied by NASA wind tunnel tests in the sixties. Their main feature is a flat surface on one side allowing for high L/D[6] if the flat surface is turned windward. After the first iteration loop six configurations were chosen for further studying. At the end of the second loop two concurring configurations were selected. After having finished the third iteration loop we now will proceed with one chosen baseline configuration.

In this paragraph we present in a concise manner the steps carried out in one iteration loop.

A. Mass Estimation

For mass estimation we relied on the DLR mass estimation tool STSM that is based on empirical relationships or user defined mass estimations for subcomponents.

The baseline configuration is equipped with the capability for autonomous de-orbiting although other alternatives are not excluded per se. In order to provide this de-orbiting capability, the vehicle is equipped with a 500 N engine fed with MMH/N2O4 fuel. In-orbit attitude control as much as attitude control during the first part of re-entry is assumed by hydrazine thrusters, preferably off the shelf. The structure itself is composed of layered TPS

on an aluminium supporting structure, the latter one responsible for supporting the mechanical loads, the former for supporting the thermal load intake. The TPS is composed of thin C/C-SiC and high temperature TPS layers. Both cover a thick layer of TPS for medium temperatures.

Due to uncertainties still remaining at this point, a global margin of 15% was added on empty mass estimations.

3D models of the vehicle were created and accommodation studies were carried out with the help of CATIA from iteration loop 2 on in order to obtain a preliminary estimation of the position of the centre of gravity necessary for stability analysis.

B. Aerodynamics and Trimming

The DLR code HOTSOSE has been employed for the evaluation of the aerodynamic characteristics and to obtain an aerodynamic data base for trajectory calculation. This code was developed for hypersonic vehicles and is based on the surface inclination method using modified Newton and shock expansion relationships. The fact that the employed method looses its validity for Mach numbers below 4 is less important to this work since much of the re-entry leg will happen for Mach numbers above this threshold.

With the help of this code, lift and drag coefficients as a function of Much number and angle of attack can be obtained for either laminar or turbulent flow. Furthermore, pitching moment coefficients related to the centre of gravity are estimated allowing for trim and static stability analysis.

A comparison with the DLR Navier-Stokes code TAU showed that the results obtained with HOTSOSE for laminar flow are in good compliance with the TAU calculations for the two flight points evaluated. The difference in L/D does not exceed 5% with HOTSOSE being slightly more optimistic[11] for the evaluated flight points. The HOTSOSE results used for this study however are those obtained with the assumption of turbulent flow resulting in the obtained L/D being about 10% less than the L/D ratios obtained with TAU code for laminar flow. We are quite confident that this approach leaves us on the save side with respect to uncertainties and with respect to the assumptions.

The results for the pitching moment coefficients are preliminary and the impact of melting ablative TPS on the nose was not considered at this point.

C. Trajectory Simulation

The calculation of the re-entry trajectory was accomplished with the TOSCA code developed by DLR. A two-staged angle of attack profile is scheduled to balance maximum heat flux versus flown L/D.

Maximum L/D is achieved for comparatively low angles of attack where lift forces are moderate. Simulations have shown though that an attitude maximizing L/D throughout the entire re-entry flight is increasing the maximum heat flux because the absolute lift in this case is insufficient to prevent a steep fall into the dense atmosphere layers when the velocities are still very important. High angles of attack on the opposite produce high lift and high drag. While high lift reduces the vertical velocity drag reduces the overall velocity. Consequently heat flux peaks are decreased. In order to meet both requirements – high L/D and low heat fluxes – a compromise has been found in choosing a two step angle of attack profile. During the initial phase of re-entry, the braking phase, a high angle of attack is assumed as with classical re-entry vehicle design in order to increase lift and drag and to reduce altitude drop. As soon as the maximum heat flux peak (occurring at the very beginning of flight through the dense atmosphere layers) passed the angle of attack is swiftly reduced to the value yielding maximum L/D.

The banking manoeuvres are used mainly to avoid skipping and to achieve crossrange if necessary. For the purpose of comparison the crossrange was kept close to zero during the first iteration loops. From the second iteration loop on the maximum crossrange was estimated by using adequate banking manoeuvres.

With the help of the DLR trajectory simulation tool TOSCA the qualitative evolution of heat flux and heat flux integral can be calculated. At this stage of study the nose radius is not yet fixed to a particular value. In order to allow comparison though, a unique nose radius of 0.01 m was assumed for all configurations.

As with aerodynamics, the impact of increasing nose radius due to melting ablative TPS material on the nose was not regarded.

IV. Results

During the first iteration loop it was aimed at developing and evaluating a wide range of configurations in order to gain a thorough understanding of relevant parameters and their impact on system level through our global system analysis approach.

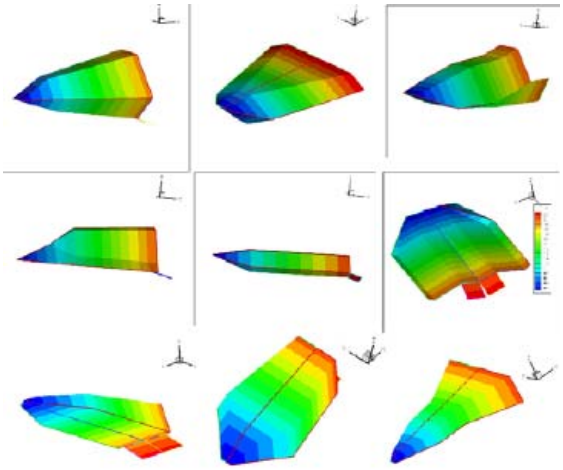

Figure 1. Selection of Rejected Configurations.

The thorough system approach led to the rejection of the major part of the examined configurations. Criteria for evaluating or rejecting configurations are:

1) Dimensions and surface (preferably small)
2) Geometric complexity (preferably low in order to keep construction effort low)
3) Overall mass (preferably low)
4) Inner volume (preferably large or at least sufficiently large to accommodate the payload container and all subcomponents)
5) Maximum heat flux peaks and integrated heat flux load (as low as possible)
6) Downrange and crossrange (as large as possible)
7) Trim capability for all flown angles of attack
8) Body flaps and body flap angle (as small as possible)
9) Aerodynamic stability (if possible)

Figure 1 presents some of the examined configurations. It shall be noted that the colour scheme has no particular significance on this figure.

Six configurations were chosen for further analysis at the outcome of which two configurations were compared with each other in terms of their performance (see Fig. 2 for one of the two configurations). For the last iteration loop one of both configurations was rejected, the other one selected for further study.

In the following section we present in detail the up-to-date results of the configuration chosen as the baseline configuration for the consecutive study.

But before we pass on to the description of the configuration we will present essential results for aspects common to all configurations. The first of these aspects are the chosen re-entry flight path angle that has a direct influence on experienced heat flux peak and on fuel consumption for de-orbiting. The second aspect concerns the subsystems and the corresponding assumptions with respect to their mass and their dimensions. This is particularly important for the accommodation study that shall result in a preliminary estimation of the position of the centre of gravity.

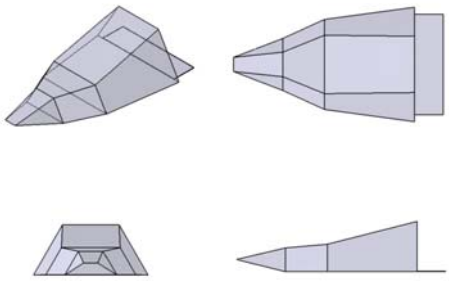

Figure 2. Rejected Configuration REX-111 after Third Iteration Loop

A. Re-entry Flight Path Angle

The re-entry flight path angle at an altitude of 120 km is of the utmost importance with respect of heat flux experienced by the vehicle during re-entry. Furthermore, steeper re-entry flight path angles will reduce downrange considerably and they will increase the propellant amount necessary for de-orbiting. These reasons lead to the preference of less steep re-entry flight path angles although these are accompanied by an increased cumulative heat load due to the increased flight times. It is obvious from these considerations that a good compromise between, fuel consumption, heat flux peak, heat flux load and downrange has to be found.

Initial Altitude H [km]	120
Reentry Flight Path Angle γ [deg]	-1.744
Relative Velocity Vrel [m/s]	7422.2
Inclination i [deg]	30
Relative Initial Azimuth / North Az [deg]	121.8
Longitude λ [deg]	60
Latitude β [deg]	0

Table 1. Re-entry Conditions for Comparison Reasons

Figure 3 shows the fuel consumption necessary for the de-orbiting from a 300 km circular orbit as a function of the vehicle MECO mass and the perigee altitude of the descent orbit. Lower perigees will correspond to steeper re-entry flight path angles.

For the purpose of comparison, the same re-entry conditions for each configuration were chosen for the iteration steps before down selection. The reason for this was to have a good comparison basis in order to choose the configuration with the best down- and crossrange capacity. This is by no means the final choice though. In the next iteration loop to be done the re-entry conditions are to be optimized.

Table 1 shows the re-entry conditions used. The re-entry position is arbitrary and shall be revised in the future when the whole mission from launch to descent initiation / splash down is analyzed. The arbitrary choice of these values is justified by the fact that at this stage of the study comparisons between different concepts in terms of their flight performance are of the main interest.

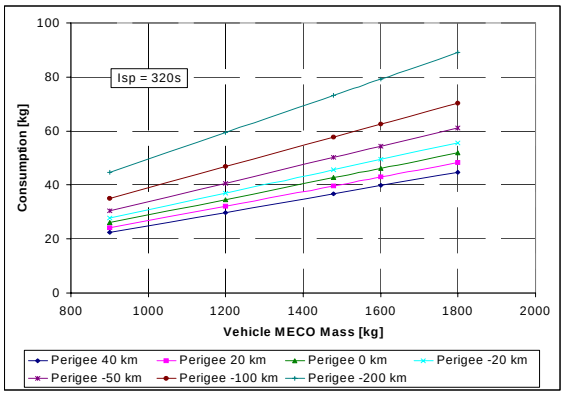

Figure 3. Fuel Mass Consumption for De-Orbiting Boost as Function of MECO Mass and of Perigee Altitude

B. Subsystems and Accommodation

In order to estimate mass and centre of gravity it is essential to have a good understanding of necessary subsystems and their position in the body. Since the mission and the operational requirements are independent of the external shape the component list is identical for each of the examined configurations. Solely their mass may vary depending on the overall vehicle mass, fuel mass and others.

The components and their estimated masses taken into account for the last two configurations are listed in table 2. A margin of 15% is added for each item.

For trimming purposes it is advantageous to approach the centre of gravity to the aerodynamic centre in order to limit flap deflection angles. In order to achieve benign longitudinal stability behaviour it is preferable to obtain a centre of gravity in forward position compared to the aerodynamic centre resulting in stable behaviour. In order to achieve these goals it is attempted to place the heaviest components as forward as possible in order to move the centre of gravity forward as much as possible. This is limited by the fact that the space delimitated by the nose walls itself is narrow and that the TPS thicknesses at the nose are very important narrowing further the available space.

At the same time the payload container shall be thus positioned that its centre of gravity coincides with the vehicle centre of gravity during orbital flight so that high quality μ-gravity conditions can be achieved independently on in-orbit manoeuvres.

Additionally, the parachute system also should preferably be located close to the centre of gravity so that the expendable cover area remains comparatively small.

Subsystem/Component	Mass [kg]
Structure	Depending on vehicle
Thermal Protection System	Depending on vehicle
Secondary Structure	25
Body flaps	Depending on vehicle
Flap Support	7.5
Flap Control Unit	34
Thrust frame OMS	20
OMS Engine	12
RCS (Engines + Tanks)	Depending on vehicle
Electrics	Depending on vehicle
Power	43
Power Control Unit	5
GNC Equipment	8
Data Handling System	32
Descent System	181
Thermal Control Unit	50
Other	75

Table 2. REX Subsystems for Mass and CoG-Estimations

C. REX-203

REX-203 whose external shape was developed by the Institute of Aerodynamics and Flow Technology[12] is the concept retained as the baseline configuration for the last iteration loop. Its bottom surface is flat allowing for high L/D. The concept was selected as it showed a good compromise in L/D, downrange and cumulative heat load.

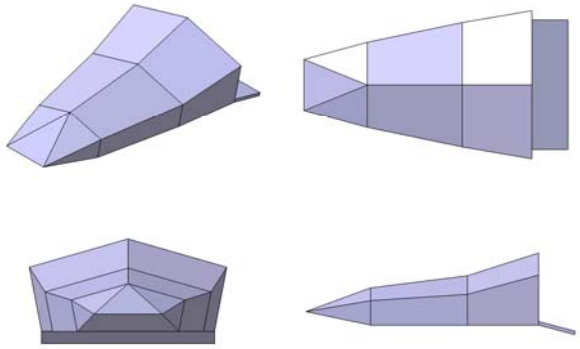

Figure 4. REX-203 Geometry

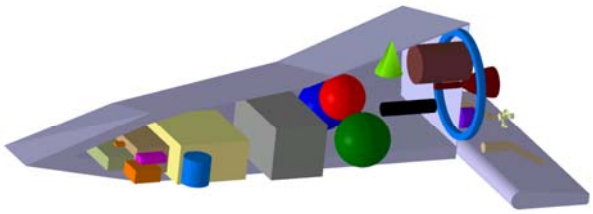

Figure 5. REX-203 Internal Accommodation

Table 3 presents the overall dimensions for the REX Free Flyer configuration.

The global take-off mass for this vehicle is estimated to 1227 kg and the longitudinal centre of gravity during re-entry is currently located at 63.2% of the length of the vehicle.

Overall Length w/o Flaps [m]	3.36
Maximum Width [m]	2.22
Maximum Height [m]	1.05
Flap Length [m]	0.54
Flap Width (one flap) [m]	0.97

Table 3. Dimensions of REX-203

Figure 6 shows the evolution of the L/D ratio with growing angle of attack and Mach number. The maximum of 2.0 is achieved for an angle of attack of 16° and a flap angle of 10.4° necessary for trimming at this flight attitude. This angle of attack will be chosen for the major part of the re-entry flight in order to achieve maximum downrange and crossrange.

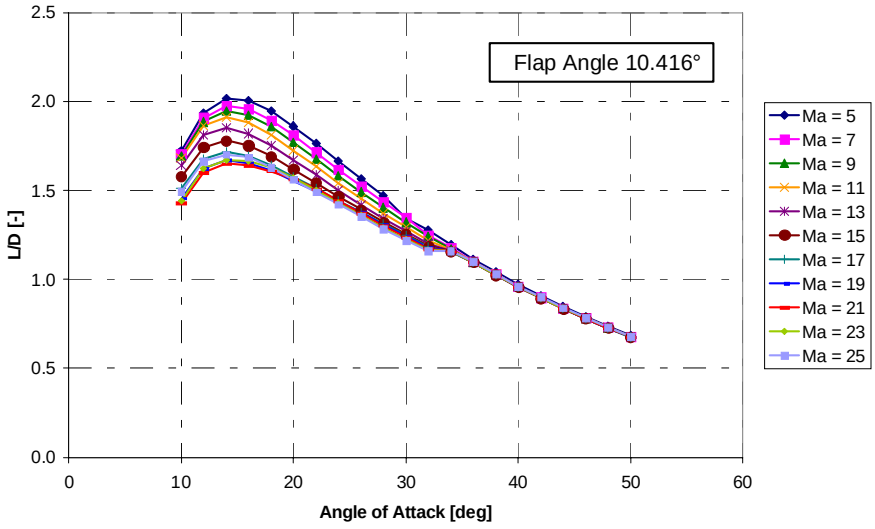

Figure 6. REX-203 Lift-to-Drag Ratio for Flap Angle of 10.4°

Attitude during the first portion of re-entry will be controlled by the reaction control system until the aerodynamic forces are large enough to take over. From this point attitude is aerodynamically controlled by the split body flap system. Therefore trim capacity has to be guaranteed and stability preferred for the attitudes assumed by the vehicle during re-entry.

As a consequence a stability and trim analysis for the degree of freedom around the lateral axis (pitching) was performed for the angle of attack of 50° and 16°.

Figures 7 and 8 show that the configuration can be trimmed and is stable for the two interesting attitudes in hypersonic flow. The given flap angles are indicative and strictly speaking only adapted each for one particular Mach number. It is obvious that the flap angle has to be constantly adapted to the Mach number in order to reduce the aerodynamic moment to zero. No vicious behaviour in terms of longitudinal stability is expected throughout the hypersonic and supersonic flight though. Stability and trimming capacity during supersonic (Ma < 5) and subsonic flight as much as lateral behaviour have yet to be analysed.

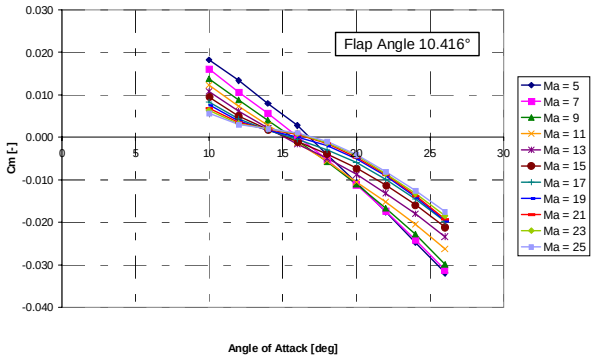

Figure 7. REX-203 Pitch Coefficient for Body Flap Angle η = 10.4° for Trimming at AoA = 16°

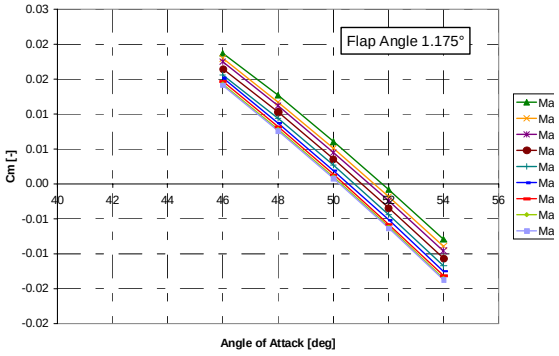

Figure 8. REX-203 Pitch Coefficient for Body Flap Angle η = 1.2° for Trimming at AoA = 50°

The flown manoeuvres lead to the profile of achieved L/D as depicted in Figure 9. Apart from the very first minutes down to Mach 26 where the flown angle of attack is 50° and the L/D small as a consequence, the achieved L/D is always above 1.6 for Mach numbers above 5 and reaches a maximum of 2 for Mach 5.

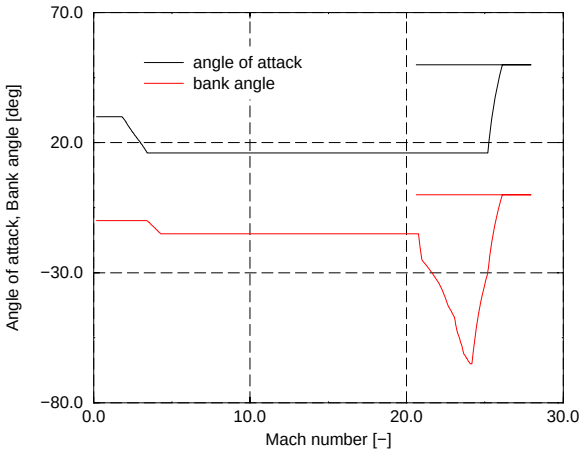

Figure 9. REX-203 Flown Angle of Attack, Banking Manoeuvers

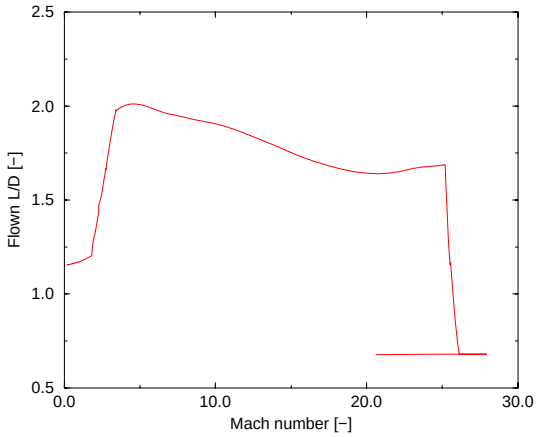

Figure 10. REX-203 Flown L/D during Re-entry

For comparison purpose a nose radius of 1 cm common to all vehicles was assumed. Nevertheless, this procedure allows comparative statements for each vehicle and optimization of flight parameters seeking to minimize both parameters. Figure 11 presents the representative heat flux and heat load obtained for REX-203 for a nose radius of 1 cm.

The achieved maximum downrange and maximum crossrange measured from re-entry position to position at end of simulation are presented in Table 4.

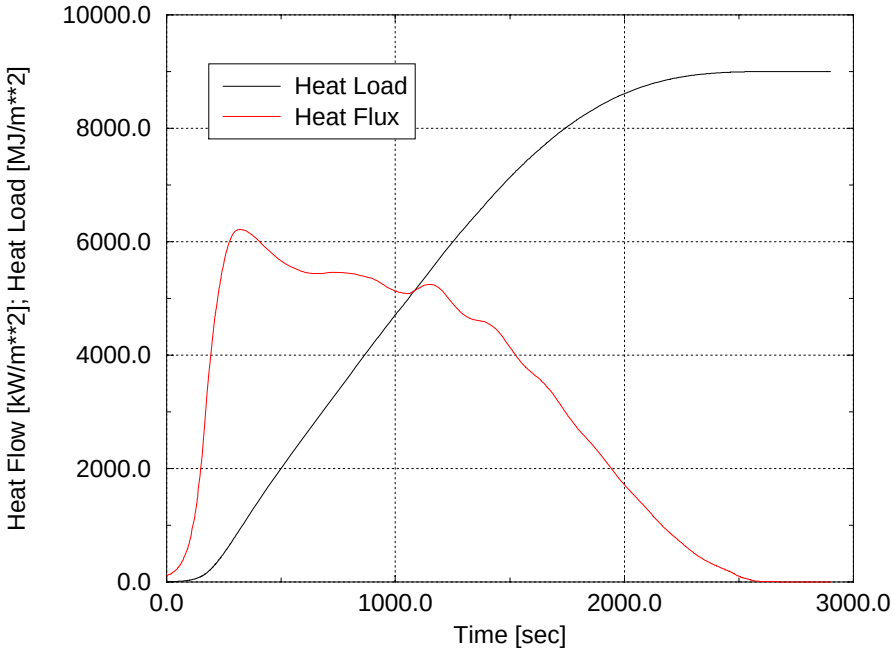

Figure 11. REX-203 Qualitative Heat Flux and Heat Load during Re-entry

Figure 12 shows the ground tracks for the trajectories maximizing the downrange and for maximum crossrange either to the north or to the south.

Max. Downrange	12300 km
Max Crossrange	2440 km

Table 4. Maximum Down- and Crossrange for REX-203

Increased banking to one side in order to deviate the trajectory for crossrange generation reduces the vertical component of the aerodynamic force leading to a reduced flight time. At the same time the altitude will decrease where banking was increased leading to higher heat fluxes. Nevertheless, simulation runs showed that the maximum heat flux occurring at the very beginning of the atmospheric flight is only slightly impacted. It is quasi identical to the trajectory generating maximum downrange when heading north. It increases slightly by 1% when heading south due to Earth rotation effects.

Due to the shortened flight time, the cumulative heat load is not negatively affected. It remains nearly identical for the north bound trajectory compared to the maximum downrange generating trajectory. It decreases significantly by 9% for the south bound trajectory.

Figure 12. REX-203 Example Re-entry Ground Tracks for Maximum Downrange and Maximum Crossrange

V. Conclusion

This article presents the current state of work for the REX Free Flyer study. For sharp-edged re-entry bodies high lift-to-drag ratios up to 2 and likely beyond are possible. Future work is scheduled to treat following aspects:

1) Calculation of aerodynamic characteristics for Mach numbers below 5
2) Analysis of stability and trim capability for Mach numbers below 5
3) Analysis of lateral stability and trim
4) Design and feasibility of thermal protection system
5) Consolidation of the structural and mass model
6) Re-iteration
7) Optimization of re-entry interface conditions
8) End-to-end trajectory simulation including Vega ascent trajectory and in-orbit phase

Beyond these points, the System Analysis Group for Space Transportation in DLR develops stochastic simulation methods in order to analyse the REX-configuration taking into account trajectory effects, aerodynamics and accommodation[9]. This method shall allow identifying promising approaches for design improvement.

Acknowledgments

The authors would like to thank J. M. A. Longo, T. Eggers and T. Barth from DLR Braunschweig for their support concerning the development of a feasible aerodynamic shape and H. Weihs from DLR Stuttgart for the structural analysis and the first designs of a TPS system.

References

[1]Essmann, O., Siemer M., Longo, J. M. A., and Weihs, H., "REX-Free Flyer: A Reusable Orbital Return Vehicle for Experiments Under Microgravity Conditions", IAC-08-A2.5.08, Glasgow, 2008.

[2]Arianespace, "VEGA User's Manual issue 3, revision 0", March 2006

[3]Reimer, T.; "Rex Free Flyer – Thermalschutzsystem Vorauslegung", DLR-IB 435-2009/15, DLR Institut für Bauweisen und Konstruktionsforschung, March 2009

[4]Kopp, A., Dietlein, I., Sippel, M., „Rex Free Flyer – Systemvorentwurf Zwischenbericht", SART TN-005/2009, DLR Institut für Raumfahrtsysteme, August 2009

[5]Brooks, C. W., Jr., Trescot, C. D., Jr., "Hypersonic aerodynamic characteristics of four series pf blunt lifting bodies and winged reentry configurations", NASA-TM-X-977, Langley Research Center, July 1964

[6]Armstrong, W. O., "Hypersonic aerodynamic characteristics of several series of lifting bodies applicable to reentry", NASA-TM-X-536, Langley Research Center, June 1961

[7]Kopp, A., "Verbesserung des HOTSOSE-Codes auf Version 1.81", SART TN-004/2009, DLR Institut für Raumfahrtsysteme, July 2009

[8]Dietlein, I., "Voruntersuchung des Wiedereintritts des REX Free Flyers (REX-111) zur Vordimensionierung des Thermalschutzsystems", SART TN-06/2009, DLR Institut für Raumfahrtsysteme, June 2009

[9]Koch, A., "Stochastic Variation of a Sharp-Edged Reentry Vehicle", AIAA-2009-7428, 16th AIAA/DLR/DGLR International Space Planes and Hypersonic Systems and Technologies Conference, Bremen, October 2009

[10]Sippel, M., Weihs, H., Barth, T., "Systematic Assessment for Advanced Sharp-Edged Lifting Body Reentry Configurations", IAC-09-D2.3.9, 60th International Astronautical Congress, Daejong, Republic of Korea, October 2009

[11]Kopp, A., Dietlein, I., Barth, T., "Systemanalyse für scharfkantige Wiedereintrittsfahrzeuge", Deutscher Luft- und Raumfahrtkongreß 2009, Aachen, September 2009

[12]Barth, T., "Aerothermodynamische Voruntersuchung der REX-Free Flyer Konfiguration", Internal Report, DLR Institut für Aerodynamik und Strömungstechnik, September 2009